Supplementary Data

The pneumococcal iron uptake protein A (PiuA) specifically recognizes tetradentate Fe^{III} *bis*- and mono-catechol complexes

Yifan Zhang[1,2], Katherine A. Edmonds[1], Daniel J. Raines[4], Brennan Murphy[1], Hongwei Wu[1], Chuchu Guo[3], Elizabeth M. Nolan[3], Michael S. VanNieuwenhze[1], Anne-K. Duhme-Klair[4] and David P. Giedroc[1,2]

[1]Department of Chemistry, Indiana University, Bloomington, IN 47405-7102 USA

[2]Department of Molecular and Cellular Biochemistry, Indiana University, Bloomington, IN 47405 USA

[3]Department of Chemistry, Massachusetts Institute of Technology, Cambridge, MA 02139 USA

[4]Department of Chemistry, University of York, Heslington, York YO10 5DD, United Kingdom

This file contains Supplementary methods, Supplementary Table 1, Supplementary Figures 1-12, and Supplementary references.

Supplementary methods

Preparation of (±)-6-Fluoronorepinephrine (6-FNE) oxalate

All non-aqueous reactions were conducted in an argon atmosphere using standard Schlenk techniques for the exclusion of moisture and air. Analytical thin layer chromatography was performed on EMD Silica Gel 60 Å 250 µm plates with F-254 indicator. ^{1}H and ^{19}F 1D spectra and 2D ^{1}H-^{1}H COSY were recorded on a Varian 400 MHz Inova NMR Spectrometer equipped with room temperature broadband probe (Supplementary Fig. 12). Mass spectra were performed by the analytical division at Indiana University Bloomington. TLC stains for visualizations of particular functional groups. $FeCl_3$ = iron trichloride: selectively stains phenols dark purple/black on a yellow background. DNP = dinitrophenylhydrazine: selectively stains aldehydes orange/red on a yellow background. CAM = ceric ammonium molybdate: general stain that is dark blue on light blue background. PMA = phosphomolybdic acid: general stain that is dark green on light yellow background. Ninhydrin: selectively stains amines and certain acylated amines. Range of colors include purple, dark blue, light blue, orange, and brown on a colorless to brown background. The following preparations were based with some modifications on work by Kirk and co-workers and synthetic intermediates were in agreement with published spectroscopic characterizations [1-4].

2-Fluoro-4,5-dihydroxybenzaldehyde

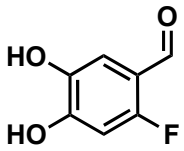

To a solution of 6-fluoroveratraldehyde (500 mg, 2.72 mmol) in dichloromethane (DCM) (15 mL) at 0 °C under argon was added BBr_3 (1.0 mL, 10.88 mmol). The reaction mixture was allowed to reach room temperature and stirred overnight. TLC indicated complete conversion to the catechol and so the reaction mixture was cooled back to 0 °C and quenched by the addition of H_2O (30 mL) and further diluted with DCM (50 mL). The organic layer was collected and aqueous layer was extracted once more with DCM (20 mL). The combined organic layers were dried over $MgSO_4$ then filtered and concentrated to an air-sensitive residue which was carried directly onto the next step (425 mg, 2.72 mmol, >99% yield). R_f = 0.25 [Hexane:EtOAc (3:1)] UV; FeCl3(+); DNP(+).

4,5-Bis(benzyloxy)-2-fluorobenzaldehyde

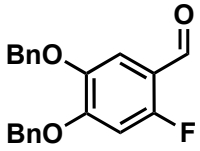

The catechol (425 mg, 2.72 mmol) and K_2CO_3 (1.50 g, 10.88 mmol) were mixed together in DMF (15 mL) then immediately treated with benzyl bromide (970 µL, 8.16 mmol) and heated to 100 °C overnight under argon. TLC showed complete conversion and so the reaction was cooled on ice and diluted with H_2O (50 mL) and Et_2O (150 mL). The organic layer was collected, the aqueous layer was further extracted with Et_2O (100 mL). The combined organic layers were washed with 1M HCl (100 mL) then brine (100 mL), dried over $MgSO_4$, filtered, and finally concentrated to provide an off-white solid residue. The residue was crystallized by dissolving in EtOAc (5 mL) then slow addition of hexane until turbidity persisted. The supernatant was removed by pipetting and solid was further washed with hexane. The material (900 mg, 2.68

mmol, 98% yield) was advanced directly to the next reaction. R_f = 0.75 [Hexane:EtOAc (3:1)] UV; $FeCl_3$ (–); DNP (+).

(±)-2-Amino-1-(4,5-bis(benzyloxy)-2-fluorophenyl)ethan-1-ol

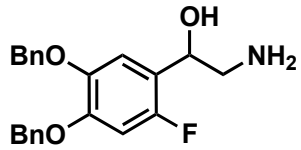

The following procedure was modified for ease of execution [5]. The 2-fluorobenzaldehyde (900 mg, 2.68 mmol) and K_2CO_3 (150 mg, 1.09 mmol) were mixed in Et_2O (15 mL) then treated with TMSCN (1 mL, 8.03 mmol) at room temperature for 24 h. When TLC indicated complete consumption of the aldehyde (Rf = 0.55 [Hexane:EtOAc (4:1)] UV; DNP; CAM; PMA), the reaction mixture was cooled to 0 °C and to it was added solid LAH (300 mg, 8.00 mmol) portion-wise to control off-gassing. After 30 minutes the reaction mixture was heated to reflux for 4 h. The reaction suspension was cooled back down to 0 °C and cautiously diluted with Et_2O (30 mL) and quenched by the dropwise addition of H_2O (300 µL). After five min, 15% NaOH (300 µL) was added and after 15 additional min H_2O (900 µL) was added. After 30 min $MgSO_4$ (2.5 g) was added and stirred for a final 10 min followed by filtration of the whole slurry through a thin Celite bed. The air-sensitive filtrate was concentrated under reduced pressure to provide a clear and colorless oil (800 mg, 2.18 mmol, 82% yield). R_f = 0.00 [Hexane:EtOAc (4:1)] UV; CAM; PMA; ninhydrin (dark blue). MS (ESI/APCI) *m/z* (M+1–18)+ calculated for $C_{22}H_{21}FNO_2$ = 350.16 Da found, 350.2 Da.

(±)-6-Fluoronorepinephrine·oxalate

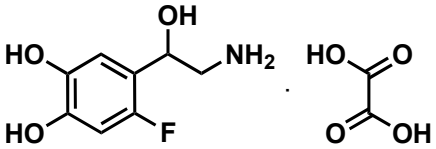

The amino alcohol (800 mg, 2.18 mmol) was dissolved in MeOH (150 mL) and to it was added $(CO_2H)2{\cdot}2H_2O$ (300 mg, 2.4 mmol) followed by Pd/C (10% w/w, 100 mg) and the headspace was purged and replaced with H_2 (balloon, 1 atm) and the reaction mixture was stirred overnight at room temperature. The Pd/C was removed by filtration through a thin bed of Celite and the filtrate was concentrated under reduced pressure to provide an air-sensitive, orange, oily residue that was precipitated by the dissolving in MeOH (2 mL) then slow dilution with Et_2O (10 mL) to provide an off-white suspension that was stored at –20 °C for 24 h. The solid was collected by mild vacuum frit filtration in the dark under an argon blanket to minimize o-quinone formation (a brown solid). The grey solid was quickly collected and stored under high vacuum at room temperature to provide an off-white solid (250 mg, 0.91 mmol, 42% yield) whose identity was confirmed by spectroscopic comparison to literature values. MS (ESI/APCI) *m/z* (2M+oxalate) calculated for $C_{18}H_{22}F_2N_2O_{10}$ = 464.12 Da, found, 465.0 Da. ^{19}F NMR (376 MHz in DMSO-d_6) characterization: δ=–130.23 (minor), –130.25 (major), –130.28 (minor) ppm.

Supplementary Table 1. SAXS structural parameters obtained for PiuA and SstD.

	apo PiuA	Fe^{III}–4-LICAM PiuA	*apo* SstD	Fe^{III}–4-LICAM SstD
R_g (Å)[a]	21.5±0.3	21.3±0.2	22.5±0.3	22.3±0.3
R_g (Å)[b]	19.9	-	20.4	-
D_{max} (Å)	75	75	72	72
MW (kDa)[c]	34.0 (31.4)	35.8 (31.6)	40.0 (35.2)	38.6 (35.4)

[a]Derived from Guinier fitting. [b]Derived from FoXS calculated SAXS from structural model. PDB Code: 4JCC for *apo* PiuA. SWISS MODEL based on PDB code: 3FGV for *apo* SstD. [c]Molecular weight calculated from SAXS; theoretical molecular weights calculated from protein sequence are shown in parentheses.

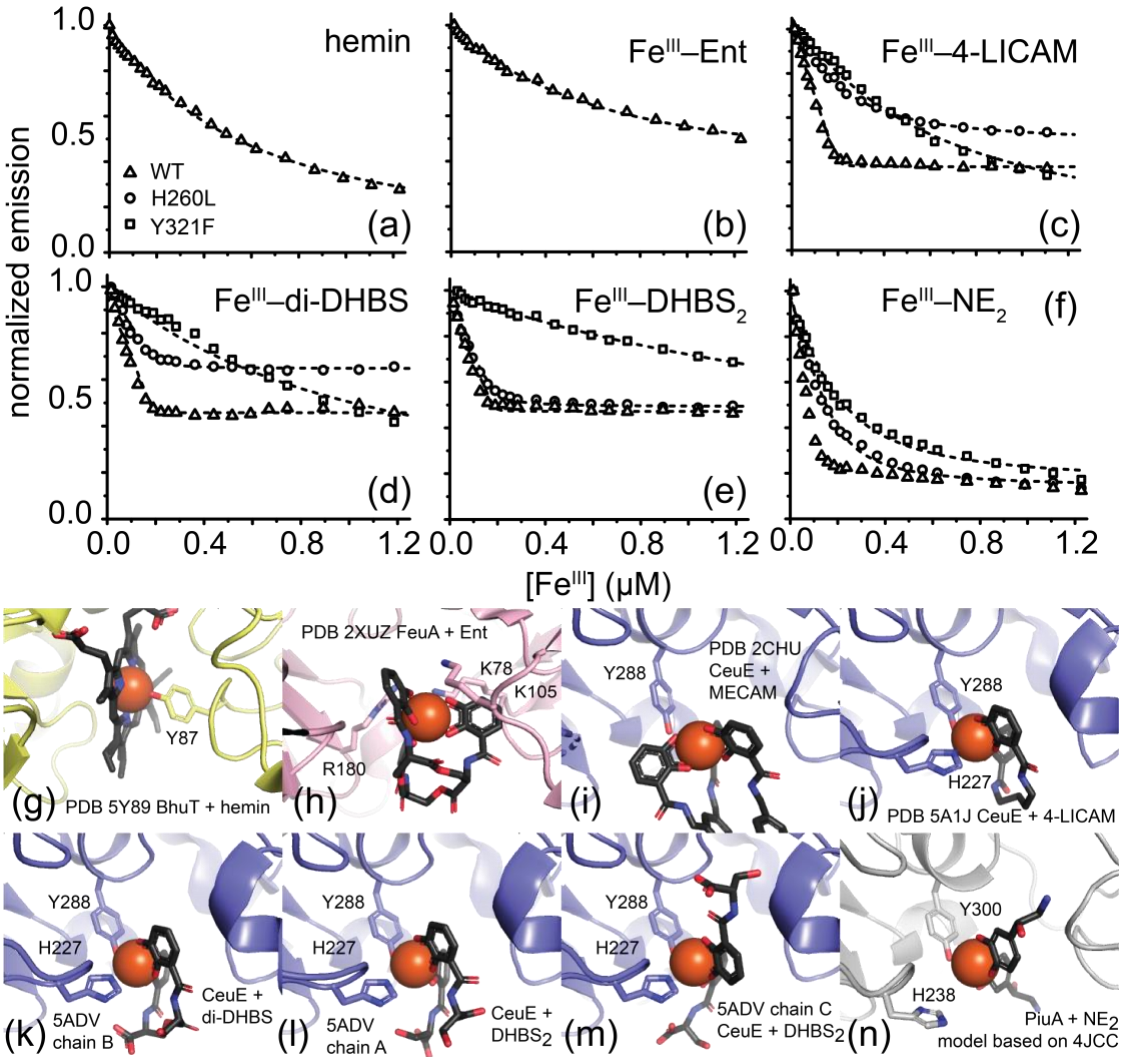

Supplementary Fig. 1. Ligand binding by wild-type *S. aureus* SstD [6] (open triangles), H260L SstD (open circles) and Y321F SstD (open squares) as monitored by quenching of the intrinsic tryptophan fluorescence. Smooth curves drawn through the data represent the results of nonlinear squares fitting to a 1:1 PiuA:ligand binding model with the parameters compiled in **Table 1** (main text). Ligands are Fe^{III} coordination complexes (a) hemin; (b) Fe^{III}–Ent; (c) Fe^{III}–4-LICAM; (d) Fe^{III}–di-DHBS; (e) Fe^{III}–DHBS$_2$; (f) Fe^{III}–NE$_2$. Conditions: 0.2 μM PiuA, 50 mM HEPES, pH 7.5, 150 mM NaCl, 25.0 ºC. Panels (g)-(m) show ribbon representations of several hemin-, enterobactin-, and catechol-binding SBPs in identical orientations, and depicting their ligands and how the ligands might be expected to bind to PiuA (n). Ligands are shown as cylinders: gray – carbon, blue – nitrogen, red – oxygen; iron – coral; ligand-binding side chains are shown as cylinders with carbon atoms colored as their ribbons. (g) PDB 5Y89 BhuT bound to hemin [7]; (h) PDB 2XUZ FeuA bound to Ent [8]; (i) PDB 2CHU CeuE bound to the non-transported enterobactin mimic MECAM [9]; (j) PDB 5A1J CeuE bound to 4-LICAM [10]; (k) PDB 5ADV chain B CeuE [11]; (l) PDB 5ADV chain A, CeuE bound to two molecules of DHBS, the hydrolysis product of di-DHBS [11]; (m) PDB 5ADV chain C, CeuE bound to DHBS in different orientations [11]; (n) Fe–NE$_2$ modeled into the apo PiuA binding site with no energy minimization (PDB 4JCC).

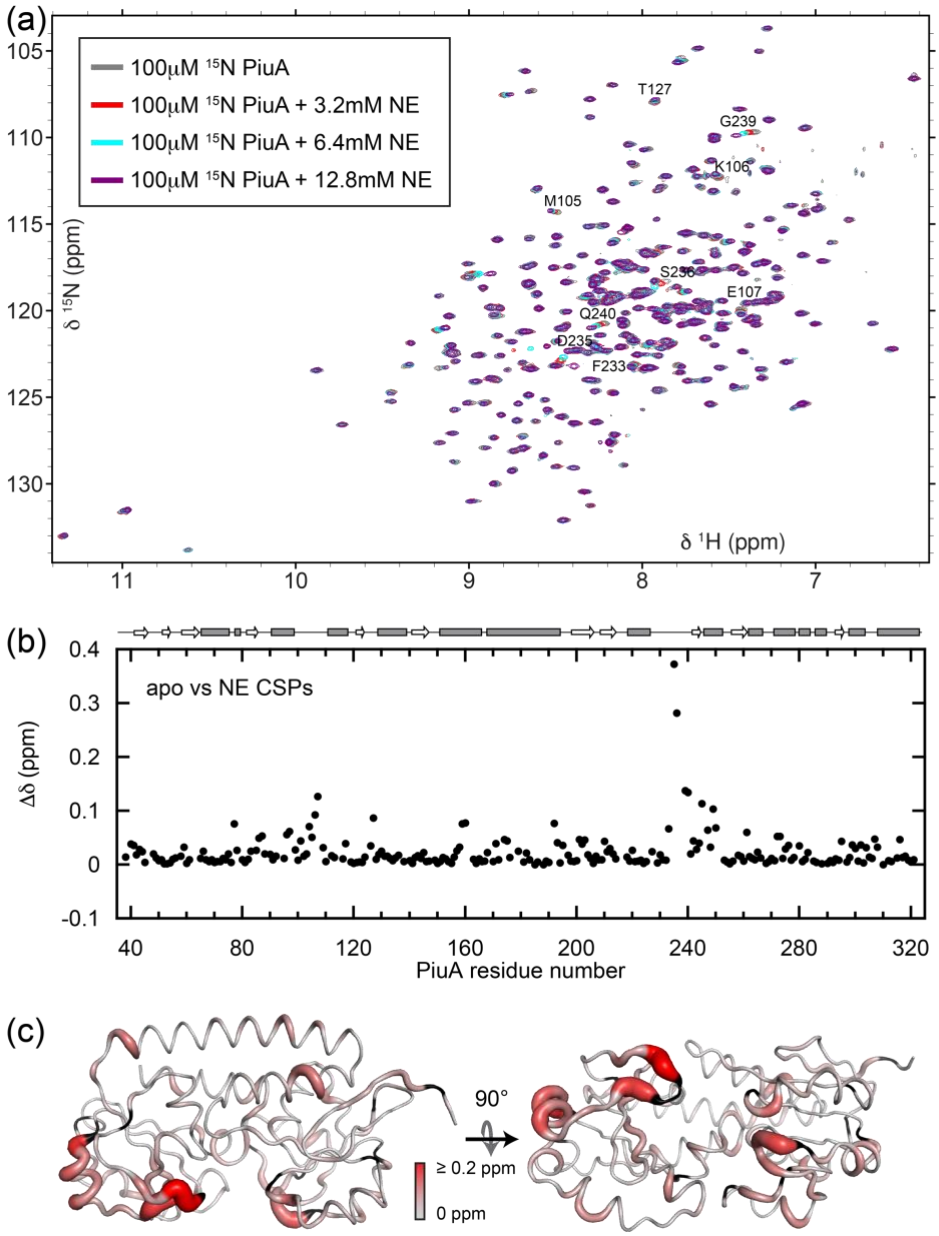

Supplementary Fig. 2. Metal-free NE binds to PiuA weakly. (a) ^{1}H,^{15}N TROSY spectrum of ^{15}N-labeled PiuA (100 μM) with no added NE (*black* contours), and 3.2 (*red*), 6.4 (*cyan*) and 12.8 mM (*magenta*) NE, with resonance assignments reported earlier [12]. (b) Chemical shift perturbation (CSP) map resulting from the addition of the 12.8 mM NE as a function of residue number, with these CSPs mapped onto the structure of the PiuA (4JCC).

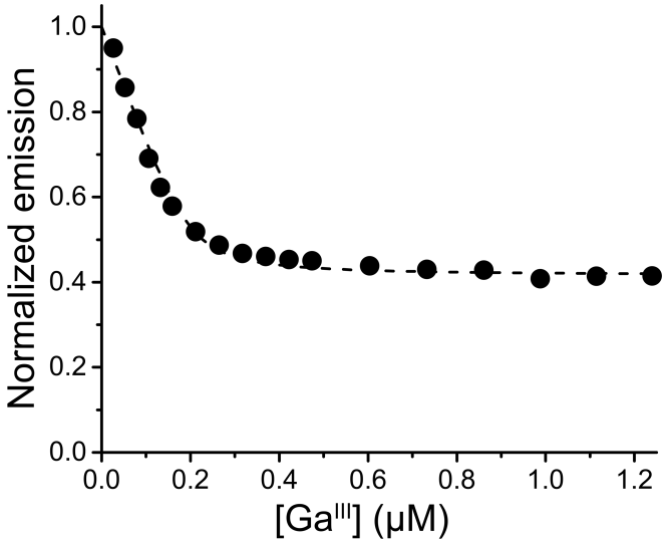

Supplementary Fig. 3. Binding of Ga^{III}-4-LICAM by wild-type PiuA as monitored by quenching of the intrinsic tryptophan fluorescence. The smooth curve drawn through the data define the results of nonlinear squares fitting to a 1:1 PiuA:ligand binding model with K_a of 1.0 (±0.2) x10^8 M^{-1}. Conditions: 0.2 μM PiuA, 50 mM HEPES, pH 7.5, 150 mM NaCl, 25.0 ºC.

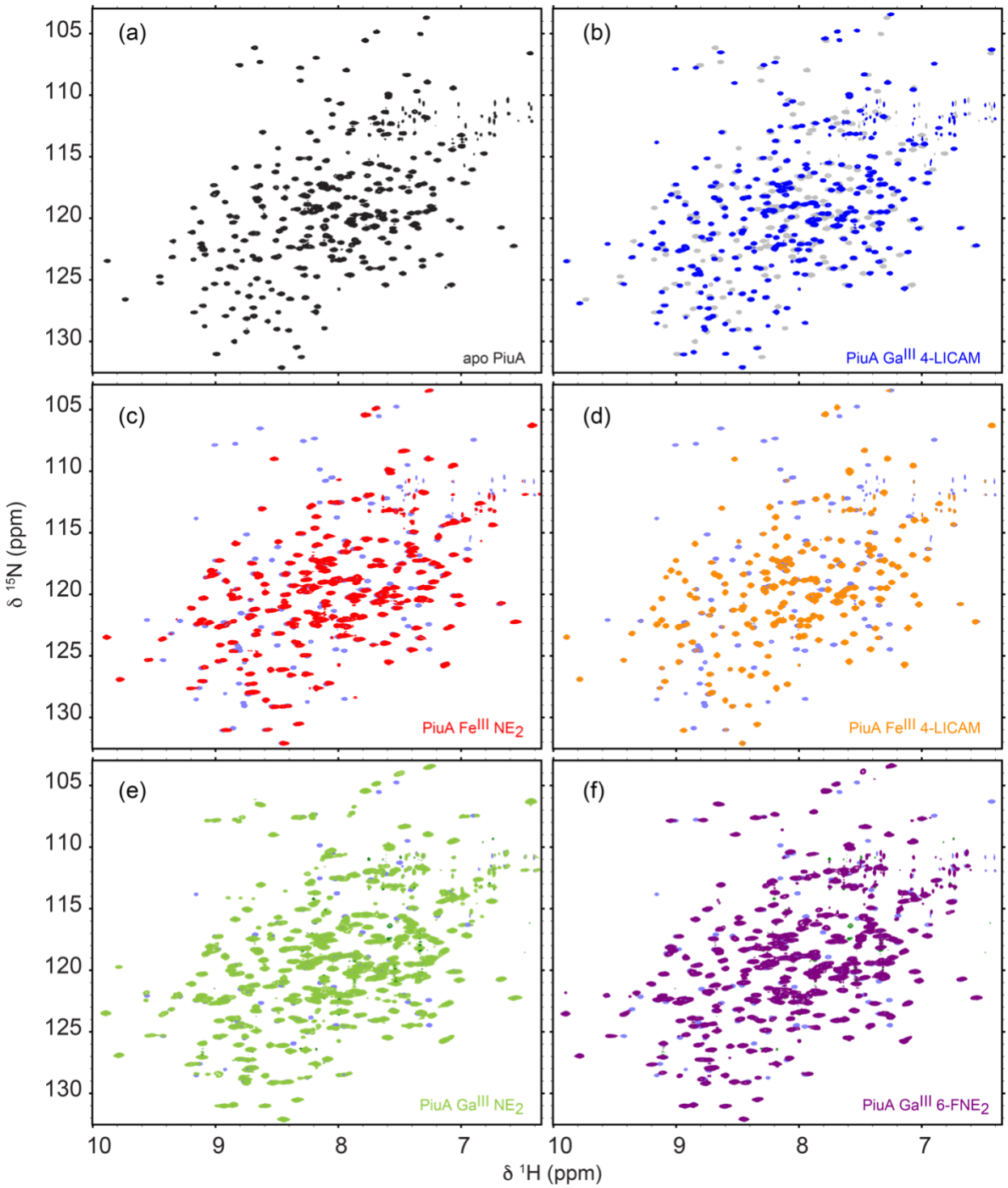

Supplementary Fig. 4. ^{1}H, ^{15}N TROSY spectra obtained for ^{15}N PiuA complexes in comparison with (a) apo PiuA: (b) Ga^{III}–4-LICAM, (c) Fe^{III}–NE$_2$, (d) Fe^{III}– 4-LICAM, (e) Ga^{III}–NE$_2$, and (f) Ga^{III}–6-FNE$_2$. For more detailed comparison, the apo spectrum is shown as overlay in gray on panel b, and the Ga^{III}–4-LICAM spectrum is shown as overlay in light blue in panels c-f. Spectral region containing the Trp indole NH crosspeaks not shown here (see Supplementary Figs. 2, 5, 6, and 9). See also ref. [12].

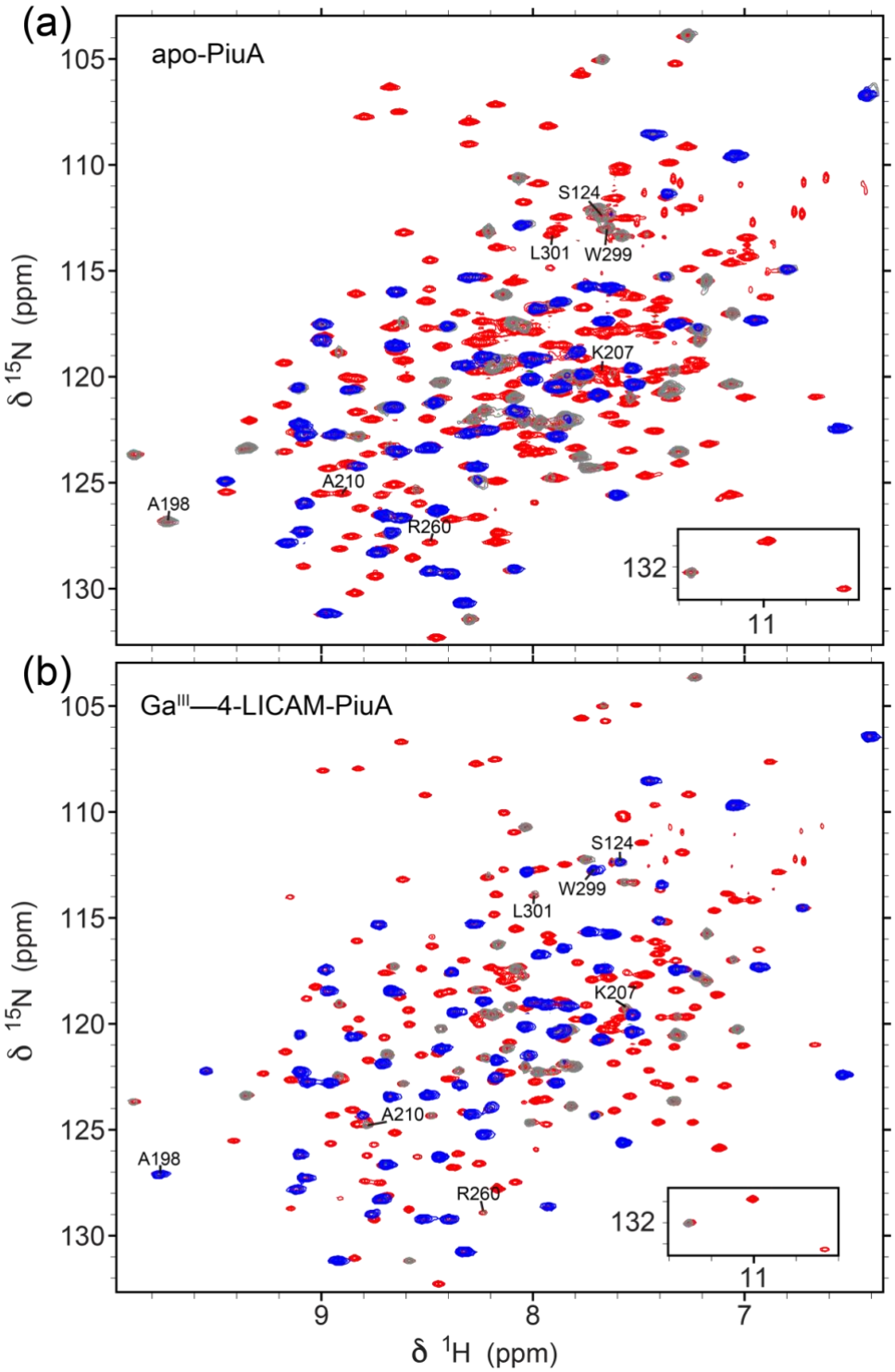

Supplementary Fig. 5. Impact of Ga^{III}–4-LICAM on amide hydrogen-deuterium exchange rates in ^{15}N PiuA. (a) ^{15}N apo-PiuA in H_2O and D_2O. (b) ^{15}N Ga^{III}–4-LICAM-PiuA in H_2O and D_2O. *Red* crosspeaks corresponding to the PiuA spectrum in H_2O are overlaid with *gray* crosspeaks, corresponding to the same spectrum after less than 1 h in D_2O, and *blue* crosspeaks correspond to those observed following 4 days in D_2O. Peaks affected by ligand binding are labeled by residue. *Insets*, Trp indole NH region.

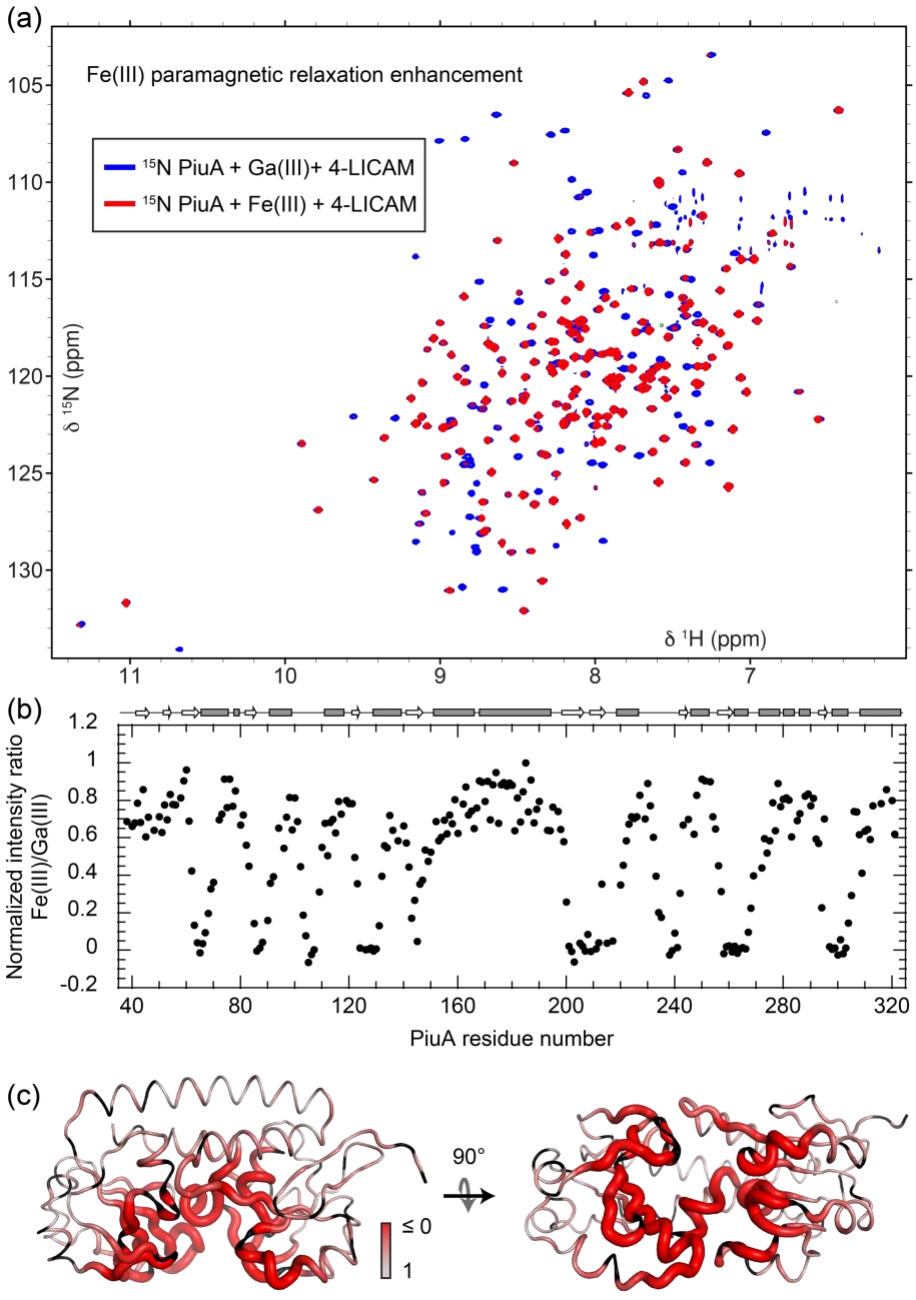

Supplementary Fig. 6. The Fe^{III}–4-LICAM and Ga^{III}–4-LICAM PiuA complexes are isostructural and collectively define the region of Fe^{III}-mediated paramagnetic relaxation enhancement (PRE). (a) Overlaid ^{15}N,^{1}H-TROSY spectra of the Fe^{III}–4-LICAM-PiuA (*red* crosspeaks) and Ga^{III}–4-LICAM-PiuA (*blue* crosspeaks) complexes [12]. (b) Normalized crosspeak intensity ratio for each backbone amide N-H crosspeak as a function of PiuA residue number, (c) mapped onto a tube diagram of the structure of *S. pneumoniae* Canada MDR_19A strain PiuA (4JCC).

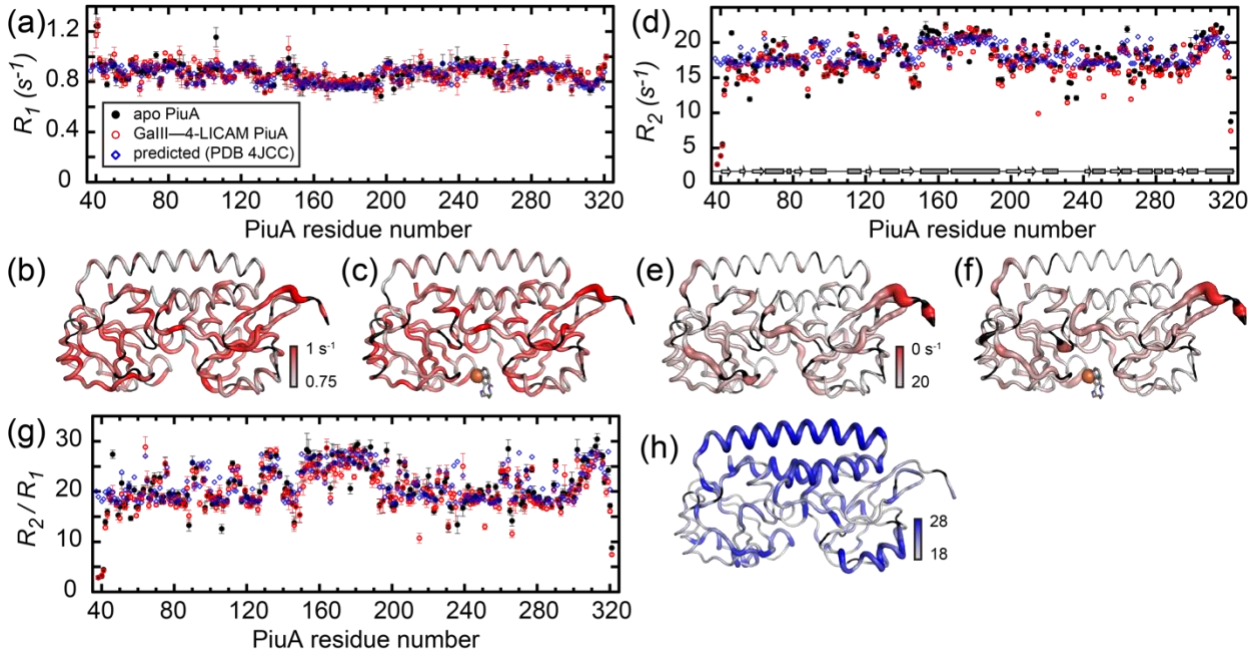

Supplementary Fig. 7. Backbone ^{15}N transverse and longitudinal spin relaxation rates of PiuA. (a) Experimental R_1 longitudinal relaxation rates for apo-PiuA (*black*) and PiuA bound to Ga^{III}–4-LICAM (*red*), with values predicted from the structure of apo-PiuA from *S. pneumoniae* Canada MDR_19A strain (PDB 4JCC) by hydroNMR (*blue*) [13]. Experimental values are depicted on a tube diagram of the structure, with the fastest relaxation shown as a thick tube painted *red*, for apo-PiuA (b) and PiuA bound to Ga^{III}–4-LICAM (c), with the substrate drawn as it appears in Fig. 1b (main text), based on the structure of the 4-LICAM-bound CeuE (PDB 5A1J) [10]. (d) Experimental R_2 transverse relaxation rates for apo-PiuA (*black*) and PiuA bound to Ga^{III}–4-LICAM (*red*), and hydroNMR predicted values (*blue*). Experimental values are depicted on a tube diagram of the structure, with the slowest relaxation shown as a thick tube painted *red*, for apo-PiuA (e) and PiuA bound to Ga^{III}–4-LICAM (f).(g) Experimental (apo *red* and Ga^{III}–4-LICAM *black*) and predicted (*blue*) values of the R_2/R_1 ratio. (h) Predicted R_2/R_1 values are painted on a tube diagram of the structure, with the highest ratio shown as a thick tube painted *blue*.

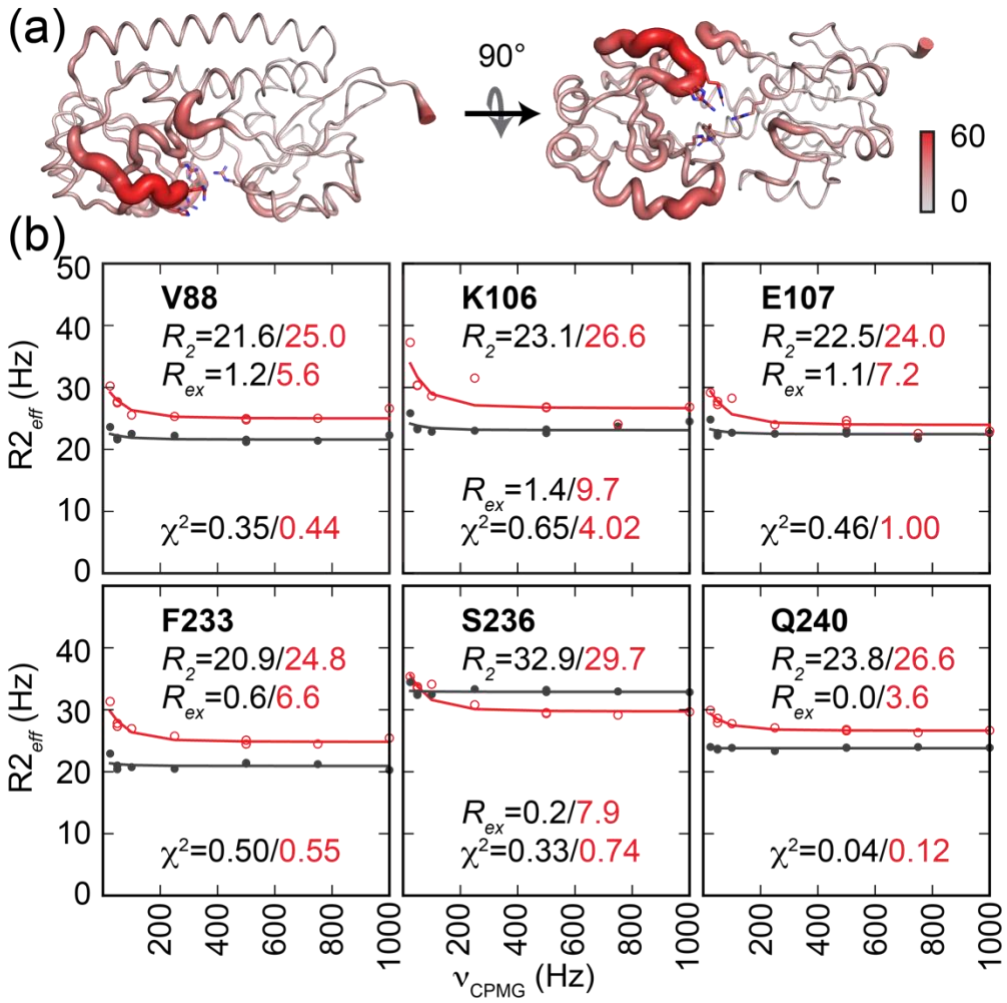

Supplementary Fig. 8. (a) Crystallographic B-factors in apo PiuA from *S. pneumoniae* Canada MDR_19A (PBD 4JCC). (b) Selected raw relaxation dispersion curves obtained for the indicated backbone amide used to obtain R_{ex} at 600 MHz, with the results for apo-PiuA shown in *black* and those for Ga^{III}–4-LICAM shown in *red*. See Fig. 6b (main text) for a compilation of data for all residues.

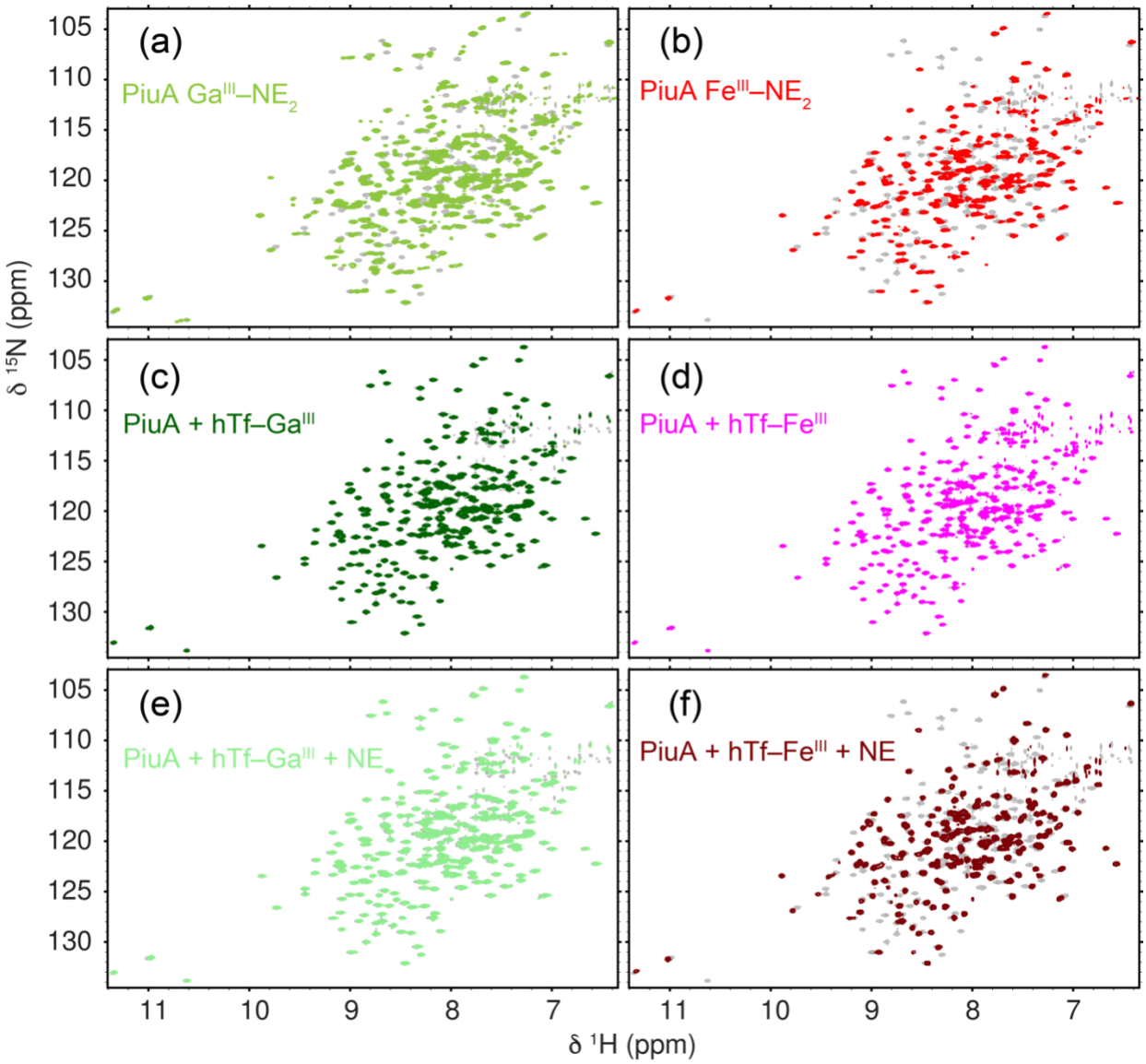

Supplementary Fig. 9. Full ^{1}H,^{15}H TROSY NMR spectra of ^{15}N PiuA showing transfer of Fe^{III} and not Ga^{III} from hTf to PiuA. (a) ^{15}N PiuA pre-loaded with Ga^{III}–NE$_2$, (b) ^{15}N PiuA pre-loaded with Fe^{III}–NE$_2$, (c) ^{15}N PiuA with Ga^{III}–hTf, showing no change, (d) ^{15}N PiuA with Fe^{III}–hTf, showing no change, (e) ^{15}N PiuA with Ga^{III}–hTf and 1 mM NE, showing no change, and (f) ^{15}N PiuA with Fe^{III}–hTf and 1 mM NE, closely resembling the spectrum shown in (b). All spectra are shown overlaid on *gray* crosspeaks corresponding to apo-PiuA. The spectral sub-regions shown in Fig. 7, panels a-f, main text are taken from these full spectra.

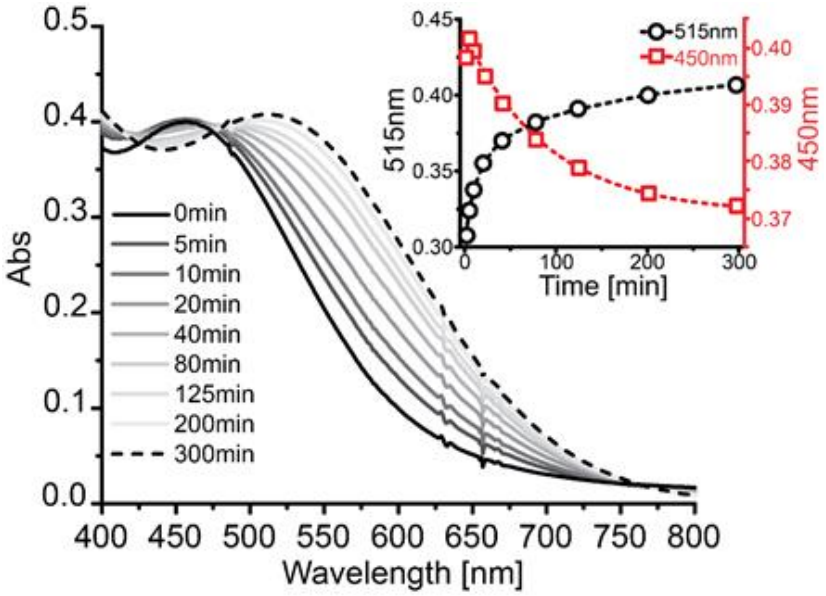

Supplementary Fig. 10. UV-Vis spectra showing NE-dependent iron transfer from hTf to PiuA over 5 h. *Inset*, absorption at 515 nm (*black*) and 450 nm (*red*), indicating the buildup of PiuA Fe^{III}–NE_2 and the decrease of hTf–Fe^{III}, respectively, over time. Exponential fittings are shown as dashed lines in the inset. The Abs_{515nm} fit a double exponential function with k_{fast}=0.082±0.004 min^{-1} and k_{slow}=0.008±0.001 min^{-1}. The Abs_{450nm} data were fit to a single exponential with k=0.011±0.001 min^{-1}.

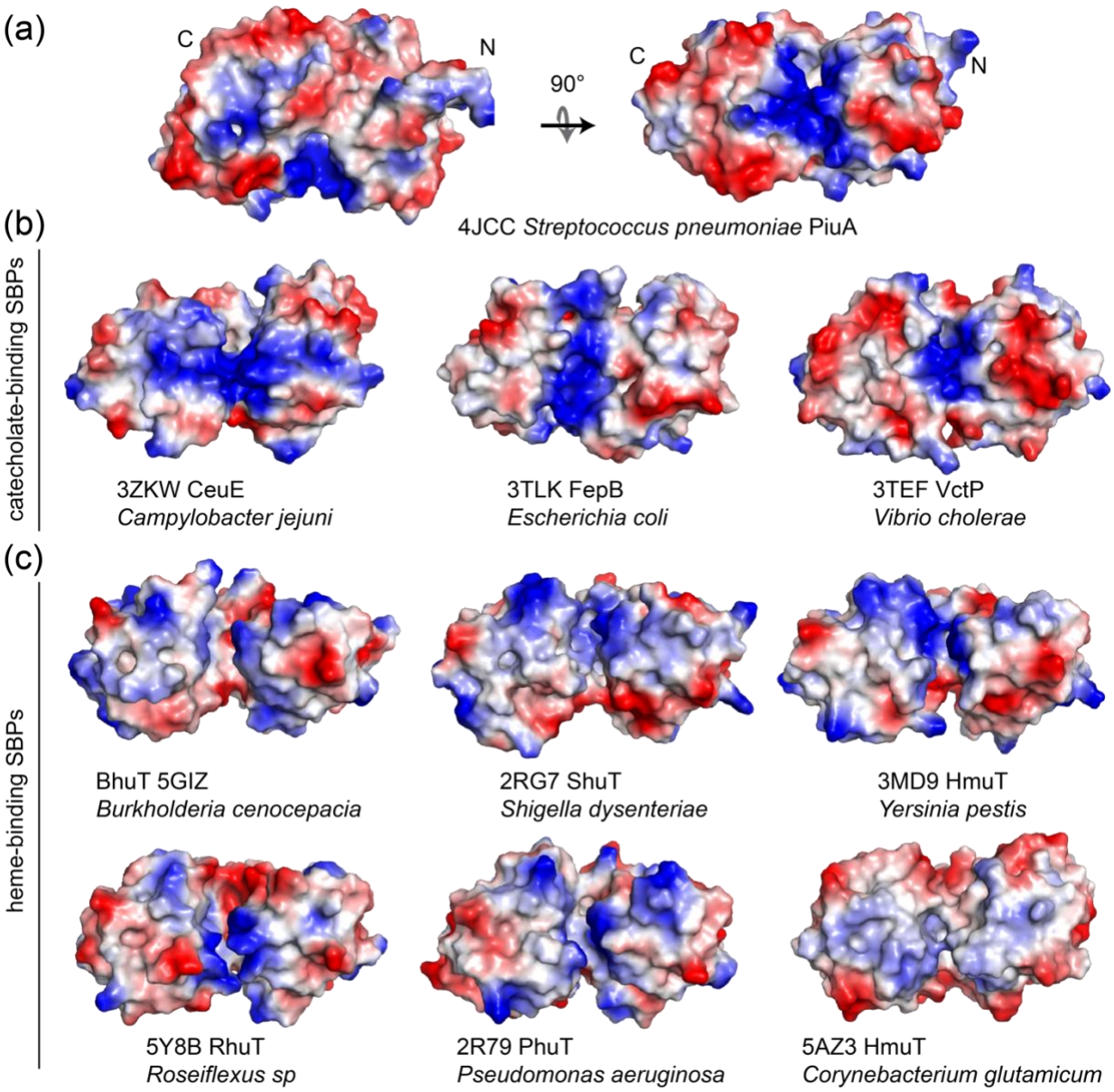

Supplementary Fig. 11. (a) Surface potential of PiuA shows a positively charged (*blue*) binding pocket between the N- and C-terminal lobes, similar to the positively charged binding pockets observed in previously characterized catecholate-binding SBPs (b), rather than the more neutral binding clefts observed in confirmed heme-binding SBPs (c) [14]. Proteins shown in panels b and c are in the same orientation as in the right side of panel a, showing the interface with the transmembrane component of the ABC transporter.

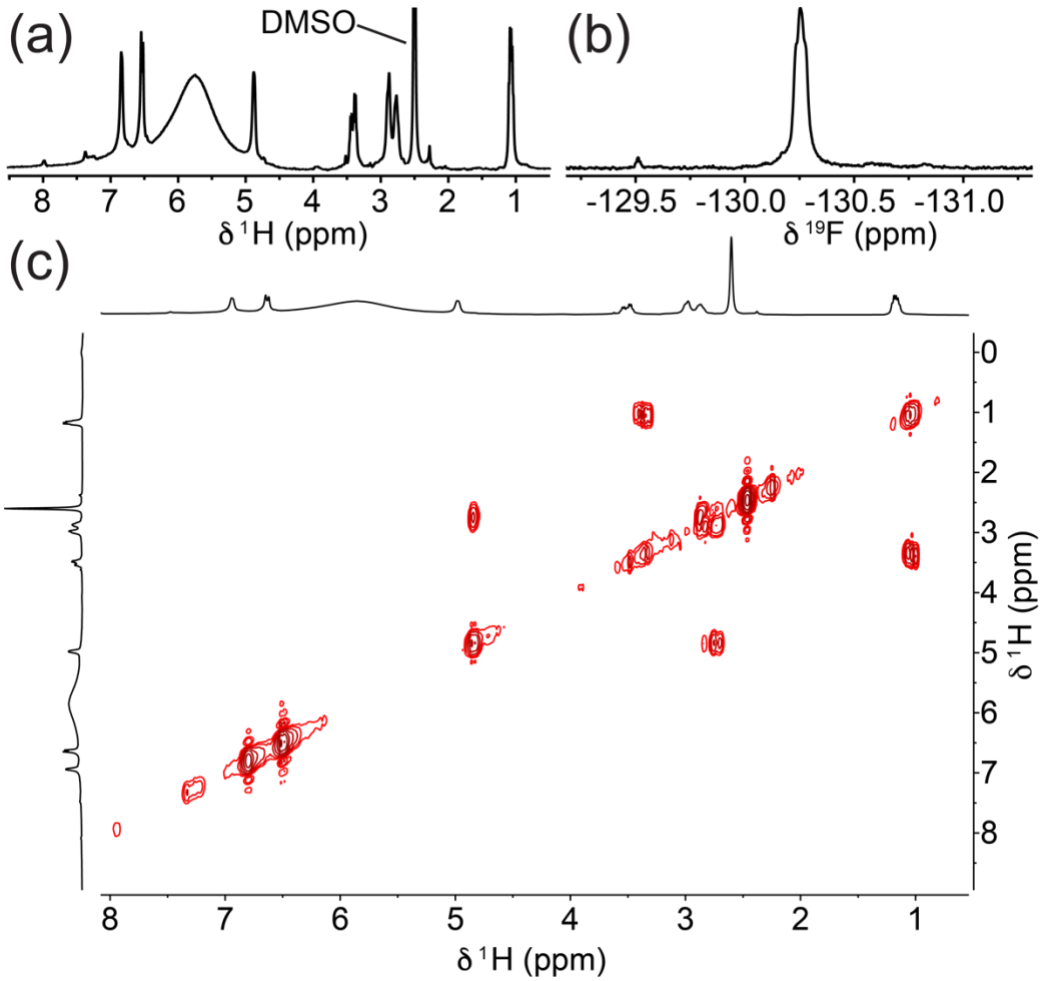

Supplementary Fig. 12. NMR spectra of 6-fluoronorepinephrine (6-FNE) in DMSO. ^{1}H (a) and ^{19}F (b) 1D spectra and 2D ^{1}H-^{1}H COSY (c), recorded on a Varian 400 MHz Inova NMR spectrometer equipped with room temperature broadband probe.

Supplementary references

[1] S.F. Lu, B. Herbert, G. Haufe, K.W. Laue, W.L. Padgett, O. Oshunleti, et al. Syntheses of (R)- and (S)-2- and 6-fluoronorepinephrine and (R)- and (S)-2- and 6-fluoroepinephrine: effect of stereochemistry on fluorine-induced adrenergic selectivities. J Med Chem 43 (2000) 1611-1619, https://doi.org/10.1021/jm990599h.

[2] K.L. Kirk, O. Olubajo, K. Buchhold, G.A. Lewandowski, F. Gusovsky, D. McCulloh, et al. Synthesis and adrenergic activity of ring-fluorinated phenylephrines. J Med Chem 29 (1986) 1982-1988, https://doi.org/10.1021/jm00160a030.

[3] K.L. Kirk, D. Cantacuzene, B. Collins, G.T. Chen, Y. Nimit, C.R. Creveling. Syntheses and adrenergic agonist properties of ring-fluorinated isoproterenols. J Med Chem 25 (1982) 680-684, https://doi.org/10.1021/jm00348a014.

[4] K.L. Kirk, D. Cantacuzene, Y. Nimitkitpaisan, D. McCulloh, W.L. Padgett, J.W. Daly, et al. Synthesis and biological properties of 2-, 5-, and 6-fluoronorepinephrines. J Med Chem 22 (1979) 1493-1497, https://doi.org/10.1021/jm00198a012.

[5] Y. Li, X. Feng, G. Zhang. Inorganic/Organic Salts as Heterogeneous Basic Catalysts for Cyanosilylation of Carbonyl Compounds. Synlett 10 (2004) 1776-1778, https://doi.org/10.1055/s-2004-829569.

[6] F.C. Beasley, C.L. Marolda, J. Cheung, S. Buac, D.E. Heinrichs. Staphylococcus aureus transporters Hts, Sir, and Sst capture iron liberated from human transferrin by Staphyloferrin A, Staphyloferrin B, and catecholamine stress hormones, respectively, and contribute to virulence. Infect Immun 79 (2011) 2345-2355, https://doi.org/10.1128/IAI.00117-11.

[7] Y. Naoe, N. Nakamura, M.M. Rahman, T. Tosha, S. Nagatoishi, K. Tsumoto, et al. Structural basis for binding and transfer of heme in bacterial heme-acquisition systems. Proteins 85 (2017) 2217-2230, https://doi.org/10.1002/prot.25386.

[8] F. Peuckert, A.L. Ramos-Vega, M. Miethke, C.J. Schworer, A.G. Albrecht, M. Oberthur, et al. The siderophore binding protein FeuA shows limited promiscuity toward exogenous triscatecholates. Chem Biol 18 (2011) 907-919, https://doi.org/10.1016/j.chembiol.2011.05.006.

[9] A. Muller, A.J. Wilkinson, K.S. Wilson, A.K. Duhme-Klair. An [{Fe(mecam)}2]6- bridge in the crystal structure of a ferric enterobactin binding protein. Angew Chem Int Ed Engl 45 (2006) 5132-5136, https://doi.org/10.1002/anie.200601198.

[10] D.J. Raines, O.V. Moroz, K.S. Wilson, A.K. Duhme-Klair. Interactions of a periplasmic binding protein with a tetradentate siderophore mimic. Angew Chem Int Ed Engl 52 (2013) 4595-4598, https://doi.org/10.1002/anie.201300751.

[11] D.J. Raines, O.V. Moroz, E.V. Blagova, J.P. Turkenburg, K.S. Wilson, A.K. Duhme-Klair. Bacteria in an intense competition for iron: Key component of the Campylobacter jejuni iron uptake system scavenges enterobactin hydrolysis product. Proc Natl Acad Sci U S A 113 (2016) 5850-5855, https://doi.org/10.1073/pnas.1520829113.

[12] K.A. Edmonds, Y. Zhang, D.J. Raines, A.K. Duhme-Klair, D.P. Giedroc. 1H, 13C, 15N backbone resonance assignments of the apo and holo forms of the ABC transporter solute binding protein PiuA from *Streptococcus pneumoniae*. Biomol NMR Assign (2020) in the press, https://doi.org/10.1007/s12104-020-09952-9.

[13] J. Garcia de la Torre, M.L. Huertas, B. Carrasco. HYDRONMR: prediction of NMR relaxation of globular proteins from atomic-level structures and hydrodynamic calculations. J Magn Reson 147 (2000) 138-146, https://doi.org/10.1006/jmre.2000.2170.

[14] P. Delepelaire. Bacterial ABC transporters of iron containing compounds. Res Microbiol 170 (2019) 345-357, https://doi.org/10.1016/j.resmic.2019.10.008.